Fe substitution in URu_2Si_2: Singlet magnetism in an extended Doniach phase diagram

Andrea Marino,[1] Denise S. Christovam,[1] Chun-Fu Chang,[1] Johannes Falke,[1] Chang-Yang Kuo,[2,3] Chi-Nan Wu,[1,3] Martin Sundermann,[1,4] Andrea Amorese,[1,5,*] Hlynur Gretarsson,[4] Eric Lee-Wong,[6] Camilla M. Moir,[7] Yuhang Deng,[7] M. Brian Maple,[7] Peter Thalmeier,[1] Liu Hao Tjeng,[1] and Andrea Severing[1,5]

[1]*Max Planck Institute for Chemical Physics of Solids, Nöthnitzer Straße 40, 01187 Dresden, Germany*
[2]*Department of Electrophysics, National Yang Ming Chiao Tung University, Hsinchu 30010, Taiwan*
[3]*National Synchrotron Radiation Research Center, 101 Hsin-Ann Road, 30076 Hsinchu, Taiwan*
[4]*PETRA III, DESY, Notkestraße 85, 22607 Hamburg, Germany*
[5]*Institute of Physics II, University of Cologne, Zülpicher Straße 77, 50937 Cologne, Germany*
[6]*Department of NanoEngineering, University of California, San Diego, California 92093, USA*
[7]*Department of Physics, University of California, San Diego, La Jolla, California 92093, USA*

(Received 23 June 2023; revised 3 August 2023; accepted 4 August 2023; published 21 August 2023)

The application of pressure as well as the successive substitution of Ru with Fe in the hidden order (HO) compound URu_2Si_2 leads to the formation of the large-moment antiferromagnetic phase. Here, we investigate the substitution series $URu_{2-x}Fe_xSi_2$ from $x = 0.0$ to 2.0 by U $4f$ core-level photoelectron spectroscopy and observe nonmonotonic changes in the spectra. The initial increase and subsequent decrease in the spectral weight of the $4f$ core-level satellite with increasing x stands for a nonmonotonic $5f$ filling across the substitution series. The competition of chemical pressure and increase in the density of states at the Fermi energy, both due to substitution of Ru with Fe, can explain such behavior. An extended Doniach phase diagram including the x dependence of the density of states is proposed. Also in $URu_{2-x}Fe_xSi_2$ the ground state is a singlet or quasidoublet state consisting of two singlets. Hence, the formation of magnetic order in the $URu_{2-x}Fe_xSi_2$ substitution series must be explained within a singlet magnetism model.

DOI: 10.1103/PhysRevB.108.085128

I. INTRODUCTION

The transition into an electronically ordered state at 17.5 K in the heavy-fermion compound URu_2Si_2 has attracted an enormous amount of interest since its discovery about 35 years ago [1–7], yet the order parameter of this phase is still a matter of debate. The small antiferromagnetic ordered moment of $0.03\mu_B$/U along the tetragonal c axis [8,9] is too small to account for the loss of entropy of about $0.2R\ln 2$ and changes in transport properties, so the presence of long-range magnetic order, charge density, or spin density wave order has to be excluded, and the name *hidden order* (HO) phase was born. The possible HO multipoles of $5f$ electrons may be classified according to the representations of U-site symmetry D_{4h}. In the quasilocalized $5f$ picture the rank-4 hexadecapole ($A_2{}^+$) order is a natural candidate [10–12]; it preserves time reversal and fourfold rotational symmetry. A superposition of a primary $A_2{}^+$ hexadecapole and subdominant $B_2{}^+$ quadrupole was proposed in [13] with broken fourfold symmetry. In the itinerant $5f$ models the rank-5 dotriacontapole which breaks time reversal is preferred [14,15]. Two candidates were considered: the twofold degenerate E^- HO, which breaks fourfold rotational symmetry [16], and the nondegenerate $A_1{}^-$, which preserves this symmetry [17]. All HO parameters are of the antiferromagnetic type with wave vector $\mathbf{Q} = (0, 0, 1)$ as in the large-moment antiferromagnetic phase (LMAFM) that appears under pressure. Furthermore, at about 1.5 K, URu_2Si_2 undergoes a second transition into an unconventional superconducting state.

In heavy-fermion compounds the hybridization of f and conduction electrons (f-d hybridization) plays a crucial role in the formation of the ground state [18–25]. How to formulate this process in uranium compounds is, however, a subject of intense discussion. Band effects are clearly important, so band structure approaches [4–6] have merit. Yet a localized $5f$ electron picture may also have value [26,27], and recently, the existence of local atomic multiplet states was observed in UM_2Si_2 (M=Fe, Ni, Ru, and Pd) [28,29]. The interplay with the bands is then represented by the noninteger filling of the $5f$ shell; that is, more than one configuration contributes to the ground state.

Motivated by the elusiveness of the HO phase, a plethora of studies explored the phase diagram of URu_2Si_2, particularly in the vicinity of the HO. The application of pressure drives the system into the LMAFM phase. At the critical pressure of $\approx$5 kbar the ordered magnetic moment rises discontinuously from $0.03\mu_B$ to about $0.4\mu_B$ [9,30–33] and aligns along the

*Present address: ASML Netherlands B.V., De Run 6501, 5504 DR Veldhoven, The Netherlands.

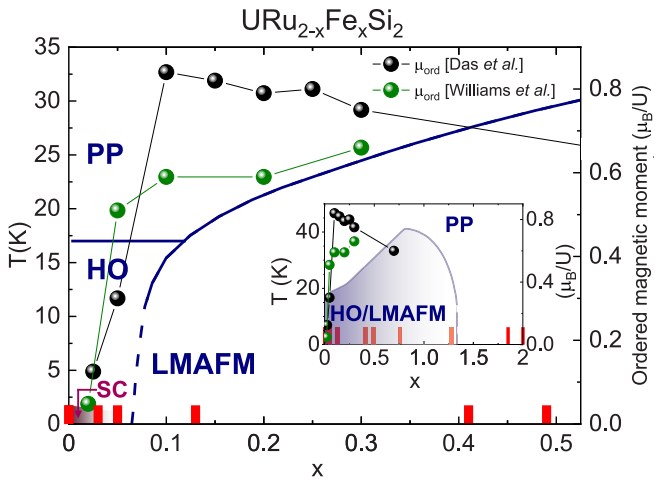

FIG. 1. Left scale: Temperature versus x, where x is the Fe concentration; the phase diagram is adapted from Refs. [41,44], showing the phase boundaries from the Pauli paramagnetic phase (PP) to the large-moment antiferromagnetic (LMAFM) and superconducting (SC) phases. Right scale: Ordered magnetic moment as measured by neutron diffraction in Refs. [39,40]. The red ticks mark the actual concentrations used in PES experiments. The inset shows the phase diagram and ordered moments over the full x range.

tetragonal c axis. It should be noted that a small orthorhombic distortion takes place for $p \gtrapprox 3$ kbar [34]. The HO phase in pristine URu_2Si_2 can also be destroyed with chemical substitution on the Ru site. Re substitution leads to ferromagnetic ordering [35], while Rh substitution favors the LMAFM phase [36–38]. Of particular interest is the isoelectronic substitution of Ru with either Fe [39–48] or Os [42,49–51], both of which drive the system from HO into the LMAFM phase, although the end members UFe_2Si_2 and UOs_2Si_2 are Pauli paramagnetic (PP) down to the lowest temperature [52–56].

Figure 1 shows the temperature vs Fe content phase diagram of the substitution series $URu_{2-x}Fe_xSi_2$ (lines) [41,44] along with the ordered magnetic moment (green and black dots) as a function of x. At first, while the moment is still increasing, the HO and LMAFM phases coexist, and the magnetic volume fraction is less than 1 [42]. The moment reaches its maximum value of about $0.8\mu_B$ according to [39] or $0.6\mu_B$ according to [40] for $x = 0.1$ with a magnetic volume of 100% [42]. As x increases further, the magnetic moment decreases, whereas the Néel temperature continues to increase up to $x = 0.8$ (see inset) and then quickly drops, reaching zero at about $x = 1.2$ [41]. For even larger x, the system enters the PP ground state of UFe_2Si_2 [52–56]. The short tetragonal a axis decreases linearly from $x = 0$ to $x = 2$, while the long c axis remains rather constant [41].

The temperature versus Fe content phase diagram of $URu_{2-x}Fe_xSi_2$ has undeniable similarities to the temperature versus pressure phase diagram of URu_2Si_2, and indeed, the resemblance was discussed for the range $x = 0$–0.3, corresponding to pressures $p = 0$–15 kbar [39,41]. Furthermore, neutron scattering experiments showed the same excitations both in the pressure and in the Fe substitution induced LMAFM phase [39,40,43], attesting to the similarity of the respective antiferromagnetic phases. In either case, the question remains open as to what causes the suppression of HO and the emergence of LMAFM. Recently, Wolowiec *et al.* [51] and Frantzeskakis *et al.* [57] pointed out the importance of changes in the $5f$-d-electron hybridization for stabilizing the LMAFM phase upon the application of pressure or substitution of Fe or Os.

Photoelectron spectroscopy (PES) is the ideal tool to study hybridization effects [58,59], so changes in $5f$-d hybridization should be observable with PES. Indeed, Fujimori *et al.* showed that the more localized compounds exhibit a stronger satellite structure in the U $4f$ core-level spectra [60,61]. This was supported by a recent core-level spectroscopy study of the UM_2Si_2 family, with M=Fe, Ru, Pd, and Ni, by some of the present authors [29] that showed that the two antiferromagnetic compounds UPd_2Si_2 [62,63] and UNi_2Si_2 [64] have a much more pronounced satellite than URu_2Si_2 (HO), which in turn has a stronger satellite than the Pauli paramagnetic compound UFe_2Si_2. With a direction dependent nonresonant inelastic x-ray scattering (NIXS) experiment, which is analogous to linear polarization dependent x-ray absorption (XAS) in its ability to determine the ground state symmetry, it was also shown that these members have the same ground state symmetry [29], namely, a singlet or quasidoublet of the U $5f^2$ configuration, so the satellite strengths in the U $4f$ core-level data are directly comparable and can be used to sort these members of the UM_2Si_2 (M=Fe, Ni, Ru, and Pd) family into a Doniach phase diagram, with temperature T versus exchange interaction $\mathcal{J}$, that describes the competition between magnetic order and a nonmagnetic delocalized state of the f electrons. For small $\mathcal{J}$, magnetic order prevails, while for large values of $\mathcal{J}$, the itinerant character of the ground state dominates. Between these two regimes, a quantum critical point occurs, and in its vicinity, superconductivity often occurs. URu_2Si_2, which is also superconducting at low T, is placed in the vicinity of the quantum critical point, the Fe compound on the side of larger $\mathcal{J}$ in the Pauli paramagnetic regime and the Ni and Pd compounds at smaller values of $\mathcal{J}$ with respect to URu_2Si_2, well in the magnetic ordering part of the Doniach phase diagram.

The present study focuses on the vicinity of the HO phase in URu_2Si_2. The substitution series $URu_{2-x}Fe_xSi_2$ is investigated with core-level PES from the HO to the LMAFM and PP phases. $URu_{2-x}Fe_xSi_2$ samples with nominal composition x that cover the entire phase diagram were measured. In Fig. 1 the *actual* compositions (see below) of the measured samples are marked by red ticks. We also present direction dependent NIXS data for single-crystalline $URu_{1.7}Fe_{0.3}Si_2$,, complementing the NIXS spectra of URu_2Si_2 and UFe_2Si_2 from Refs. [28,29].

II. EXPERIMENT

Polycrystalline samples of Fe-substituted URu_2Si_2 used in the PES experiment were prepared by arc melting in an argon atmosphere and then analyzed by x-ray powder diffraction to determine quality and stoichiometry. The actual Fe concentration, as examined by elemental analysis using energy dispersive x-ray spectroscopy, was uniform throughout the sample and in good agreement with the nominal concentration. The actual relative composition of the spots measured

TABLE I. Nominal composition compared to the composition estimated from the Fe $2p$ intensity, as normalized to the U $4d$ integrated intensity. The Fe $2p$ intensity for $x = 2$ serves as the reference composition. The labels indicate the phase: HO is hidden order, AFM is antiferromagnetic order, and PP is the Pauli paramagnetic order.

Nominal composition	Actual composition
0.00	0.00 HO
0.05	0.05 HO/AFM
0.08	0.03 HO/AFM
0.1	0.13 AFM
0.4	0.41 AFM
0.5	0.49 AFM
0.8	0.76 AFM
1.3	1.28 AFM/PP
1.8	1.85 PP
2.0	2.00 PP

with PES was also checked by comparing the intensities of the U $4d$ and Fe $2p$ core-level emission lines and was very much in agreement with the nominal composition (see Table I).

Single-crystalline $URu_{1.7}Fe_{0.3}Si_2$ used in the NIXS experiment was grown by the Czochralski method in a tetra-arc furnace from high-purity starting elements. Pieces were taken from the single-crystalline parts of the boule, and a small piece of the boule was then analyzed [43] by powder diffraction to determine structure and quality. The real Fe concentration was examined by elemental analysis using energy dispersive x-ray spectroscopy, which is uniform throughout the sample and in good agreement with the nominal concentration.

Soft x-ray PES experiments were performed at the NSRRC-MPI TPS 45A Submicron Soft X-ray Spectroscopy beamline [65] at the Taiwan Photon Source in Taiwan. The incident photon energy was set to 1200 eV. The valence band spectrum of a platinum sample was measured in order to determine the chemical potential and the overall instrumental resolution of about 200 meV. The excited photoelectrons were collected using a MB Scientific A-1 photoelectron analyzer in the horizontal plane at 60°. The sample was measured at normal emission. Clean sample surfaces were obtained by cleaving the samples *in situ* in the cleaving chamber prior to inserting them into the main chamber. In both chambers the pressure was in the low 10^{-10} mbar regime. The measurements were performed at a temperature of 40 K.

The NIXS experiment was performed at the High-Resolution Dynamics Beamline P01 of the PETRA-III synchrotron in Hamburg, Germany. The sample temperature was kept at 15 K in a vacuum cryostat. The incident energy was selected with a Si(311) double monochromator. The P01 NIXS end station has a vertical geometry with 12 Si(660) 1 m radius spherically bent crystal analyzers, fixing the final energy to 9690 eV. The analyzers are positioned at $2\theta \approx 155^o$, giving a momentum transfer of $|\mathbf{q}| \approx 9.6\text{Å}^{-1}$. The experimental energy resolution, determined by regularly measuring the elastic line, amounts to ≈0.7 eV. More details on the setup can be found in Ref. [66]. The multipole selection rules in a NIXS experiment at high momentum transfers q give access to the ground state symmetry in a fashion similar to the dipole selection rules in XAS [67,68]. In NIXS, the direction of the momentum transfer, i.e., $\vec{q}$, takes over the role of the electric field vector $\vec{E}$ in XAS. For uranium compounds, high-q NIXS has the advantage of more excitonic excitations, and the nonresonant process facilitates the quantitative modeling [28,29,69,70].

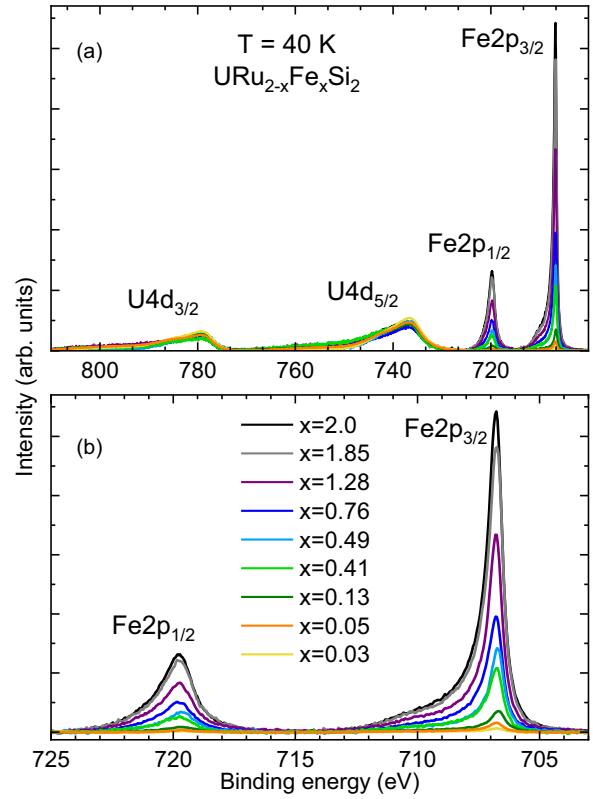

FIG. 2. (a) U $4d$ and Fe $2p$ and (b) Fe $2p$ core-level spectra of $URu_{2-x}Fe_xSi_2$. The spectra are integrated background (Shirley) corrected and normalized to the area of the U $4d$ peaks.

III. RESULTS

Figure 2(a) shows the U $4d$ and Fe $2p$ core-level spectra of $URu_{2-x}Fe_xSi_2$ after the subtraction of an integrated (Shirley) background and normalization to the integrated intensity of the U $4d$ lines. U $4d$ can be used for normalization because it is a full shell, so the PES intensities should not vary across the $URu_{2-x}Fe_xSi_2$ series. Fe $2p$ is also a full shell, so differences in its intensity must be due to the different Fe contents in the samples, making it suitable for determining the actual compositions. Figure 2(b) shows a blowup of the Fe $2p$ lines. We consider the ratio of the integrated Fe $2p$ area of a sample with Fe content x to the integrated Fe $2p$ area of the UFe_2Si_2 sample. We take the latter as a reference. The $x = 0$ sample does not show any Fe lines. We then compare the ratios to their nominal values and estimate the composition. We find that the composition of the spots measured with PES agrees well with the nominal compositions, as shown in Table I. Only the nominal $x = 0.08$ sample seems to have a slightly lower actual composition, so this sample is also still in the HO phase. In the following we refer to the actual composition.

Figure 3(a) shows the U $4f$ core-level spectra of the $URu_{2-x}Fe_xSi_2$ samples after the subtraction of an integrated

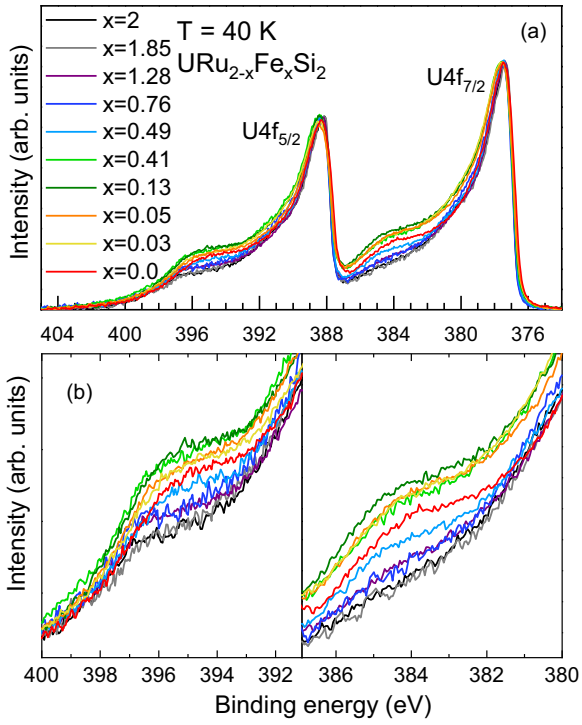

FIG. 3. (a) U $4f$ core-level data for $URu_{2-x}Fe_xSi_2$. The spectra are normalized to the main peak of the spectrum, and an integrated background (Shirley) is subtracted. (b) Blowup of the satellite regions of the U $4f_{5/2}$ (left) and U $4f_{7/2}$ (right) lines.

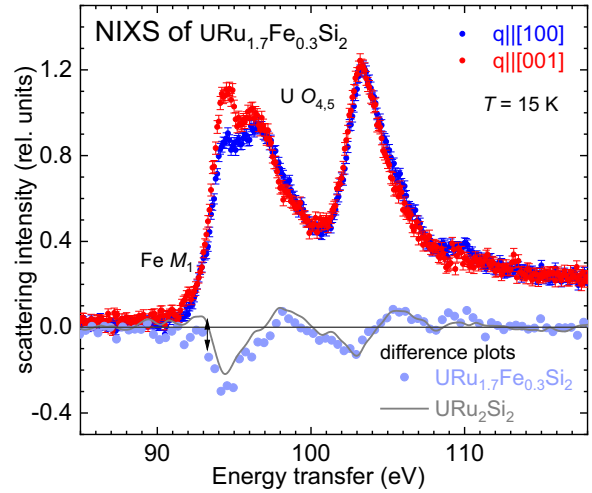

FIG. 4. Normalized and background-corrected experimental NIXS data for $URu_{1.7}Fe_{0.3}Si_2$ at the U $O_{4,5}$ edges ($5d \rightarrow 5f$) at $T = 15$ K for $\vec{q}\|[100]$ (blue dots) and $\vec{q}\|[001]$ (red dots), plus the difference plots $I_{\vec{q}\|[100]} - I_{\vec{q}\|[001]}$ (violet dots). The arrow marks the region where Fe M_1 scattering appears in the spectra. For comparison the difference data for URu_2Si_2 are shown (gray line), adapted from Ref. [28]. When no error bars are given, the size of the data points represents the statistical error.

(Shirley) background and normalization to the U $4f_{7/2}$ peak at ≈377.4 eV binding energy. The U $4f_{5/2}$ and U $4f_{7/2}$ multiplet structures are split by about 11 eV by the U $4f$ spin-orbit interaction. Both the U $4f_{5/2}$ and U $4f_{7/2}$ emission lines originate from the same mixed-valence initial state U configuration, and they both show satellite structures. The ratio of the integrated intensities of the U $4f_{5/2}$ and U $4f_{7/2}$ emission lines (main and satellite) is about 0.8, which is close to the expectation value $6/8 = 0.75$.

We are searching for changes in spectral weights as a function of substitution rather than attempting to determine the absolute occupation of the $5f$ shell. We therefore focus on the satellite structure, as shown in Fig. 3(b) for the U $4f_{5/2}$ (left) and U $4f_{7/2}$ (right) emission lines. The $x = 0$ (URu_2Si_2) satellite structure in the HO phase is much more pronounced than that of the $x = 2$ sample (UFe_2Si_2) in the PP phase, in agreement with previous findings [29]. Looking at the different compositions in detail, we find that starting from $x = 0$, the satellite first increases, peaks for $x = 0.13$, then decreases, and becomes smaller than that for URu_2Si_2 for $x \geqslant 0.49$ until it smoothly overlaps with the $x = 2.0$ spectral shape. The satellite structures of both emission lines consistently show the same trend.

Before discussing the above observation further, it should be emphasized that the comparison of PES spectra in terms of hybridization is sensible only if other changes in, e.g., ground state symmetry and/or degeneracy can be excluded. Indeed, we already know from Refs. [28,29] that the end members of the substitution series URu_2Si_2 and UFe_2Si_2 have the same symmetry, so it is reasonable to assume this is also the case for the compositions between them. For confirmation, Fig. 4 shows the U $O_{4,5}$ edge ($5d \rightarrow 5f$) NIXS data for $URu_{1.7}Fe_{0.3}Si_2$ at 15 K for two directions of the momentum transfer $\vec{q}$: $\vec{q}\|[100]$ (blue) and $\vec{q}\|[001]$ (red). Two aspects are striking, namely, the strong directional dependence and the existence of a multiplet structure. The spectral shape and directional dependence are the same as for URu_2Si_2 and UFe_2Si_2. These data show that the ground state symmetry remains the singlet $\Gamma_1^{(1)}(\theta) = \frac{1}{\sqrt{2}}\sin\theta(|+4\rangle + |-4\rangle) + \frac{1}{\sqrt{2}}\cos\theta|0\rangle$ or $\Gamma_2 = \frac{1}{\sqrt{2}}(|+4\rangle - |-4\rangle)$ or a quasidoublet constructed from these two singlet states for this intermediate Fe concentration.

IV. DISCUSSION

Uranium in intermetallic compounds usually has a strongly intermediate valence between 4+ and 3+, i.e., a configuration between $5f^2$ and $5f^3$. In previous works, it was shown that the symmetry of URu_2Si_2 is determined by the U $5f^2$ configuration, implying this is the configuration lowest in energy and that the f-level filling is closer to 2 than to 3. The degree of itinerancy can be identified as the deviation n_f from integer valence f^2; in other words, it is given by the extra participation of a third electron when following the *dual-nature* concept of f electrons as discussed for some U intermetallic compounds [71–73]. Strong satellites in the $4f$ core-level PES spectra of uranium intermetallic compounds are interpreted as a sign of strong localization [29,60,61]. Hence, within the UM_2Si_2 series where the satellites appear at the same binding energy, the satellite spectral weight is related to the occupation of the $5f$ shell, where strong satellites indicate greater f^2 and favor

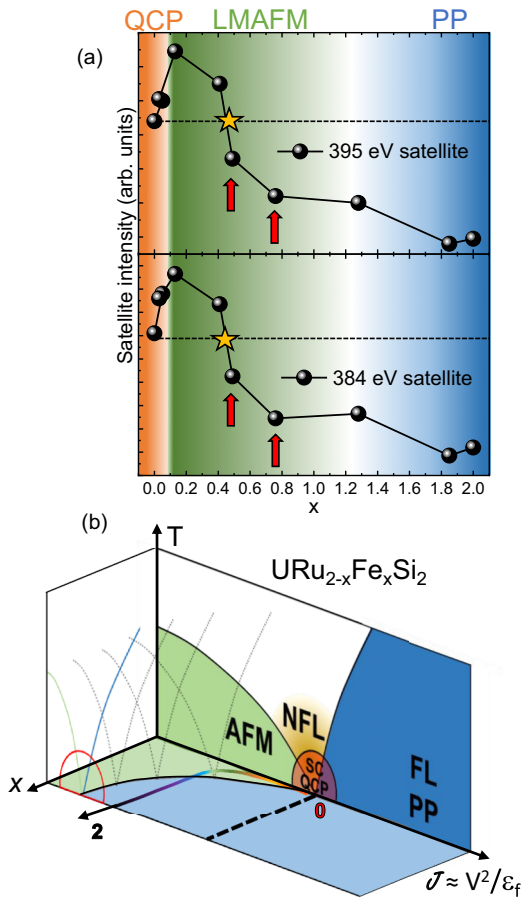

FIG. 5. (a) Satellite intensities of the U $4f$ emission spectra at 395 and 384 eV binding energy as a function of x. The red arrows indicate values of x showing a smaller satellite structure than $x = 0$, despite being in the LMAFM phase. (b) Extended Doniach phase diagram (T, $\mathcal{J}$, x) of $URu_{2-x}Fe_xSi_2$. AFM = antiferromagnetic, SC = superconducting, QCP = quantum critical point, NFL = non-Fermi liquid, FL = Fermi liquid, and PP = Pauli paramagnetic.

magnetism, while weaker satellites imply more itinerancy due to a larger contribution of a third electron (f^3 configuration) and a Pauli paramagnetic ground state.

In the $URu_{2-x}Fe_xSi_2$ series, the satellite spectral weight first increases up to $x = 0.13$, then decreases again, and becomes smaller in comparison to URu_2Si_2 for $x \geqslant 0.49$. This alternating trend in the core-level intensities (or f-electron count) comes as a surprise because there are no anomalies in, e.g., the lattice constants or cell volume as a function of x in $URu_{2-x}Fe_xSi_2$ [41]. Moreover, the satellite intensities for $0 < x < 0.4$ cannot be composed of the satellite strengths of the end members of the series. This becomes evident when looking at Fig. 5(a), where the intensities of the U $4f$ spectra at 395 and 384 eV binding energy are plotted as a function of the Fe concentration x. The background colors indicate the respective phases; the hidden order phase close to a quantum critical point (QCP) and region of phase coexistence is in orange, the magnetic (LMAFM) region is in green, and the PP phase is in blue. The horizontal dashed lines mark the satellite spectral weight of URu_2Si_2.

A. The effect of chemical pressure

The substitution of Fe in URu_2Si_2 leads to a continuous decrease of the unit cell volume so that, like for applied pressure, the configuration with the smaller ionic radius, U f^2, becomes the more favorable one. This suggests that the satellite intensity will increase. Indeed, the satellite intensity is, at first, more pronounced, thus proving that the U f^2 configuration is stabilized. However, by reducing the lattice spacings due to chemical pressure, the hybridization V of f and conduction electron states will also increase. Hence, while keeping in mind that a Kondo state is nearby, the material can reach the LMAFM phase only when the on-site exchange interaction

$$\mathcal{J} \propto \frac{V^2}{|\epsilon_f|}, \tag{1}$$

with ϵ_f being the f-level position relative to the Fermi energy [25,74], becomes smaller with chemical pressure. Here, it is assumed that URu_2Si_2, which is superconducting at low temperatures, is close to the QCP, so the AFM region can be reached with pressure only when $\mathcal{J}$ decreases. This, in turn, can happen only when the parameter $|\epsilon_f|$ increases faster with pressure than V^2. This situation is reminiscent of Yb heavy-fermion compounds in which pressure stabilizes the smaller f^{13} configuration, i.e., makes Yb more magnetic at the detriment of itinerancy, although V increases (see, e.g., [75]).

So far our findings support the similarities between the (p, T) phase diagram of URu_2Si_2 for pressures $\leqslant$15 kbar and the (x, T) phase diagram of $URu_{2-x}Fe_xSi_2$ for $x \leqslant 0.3$ [39,41] and are in agreement with the additivity of chemical and external pressures, as suggested in Refs. [41,45]. Also, Das *et al.* [39] and Kanchanavatee *et al.* [41] discussed reaching the LMAFM phase in terms of increasing V^2, but without considering the necessity of ϵ_f in the presence of a nearby Kondo state.

B. The additional effect of substitution

The satellite spectral weight decreases with a further increase of x and eventually becomes smaller than that in URu_2Si_2. This could suggest that now $\mathcal{J}$ is increasing with x. However, $URu_{2-x}Fe_xSi_2$ is still magnetic despite the smaller satellite between $x \approx 0.4$ and $x \approx 1.2$ [see red arrows in Fig. 5(a)]. If the satellite strength, and with it the f-electron count, were driven by only $\mathcal{J}$, we would then rather expect a QCP where the satellite spectral weight of URu_2Si_2 is recovered [see yellow star in Fig. 5(a)]. This satellite strength would denote the quantum critical value of the exchange interaction $\mathcal{J}_c$. That is, however, not the case: the yellow star still lies in the LMAFM regime. We would further expect a Pauli paramagnetic regime for the entire region with satellites smaller than in URu_2Si_2, i.e., also for the concentrations marked by the red arrows in Fig. 5(a). A dilemma is then posed. It cannot be solved even if we were to further speculate that $\mathcal{J}$ itself has a nonmonotonic behavior: even if $\mathcal{J}$ increased, after its decrease at low x due to chemical pressure, we would never expect antiferromagnetic order to occur for any Fe concentration with a satellite smaller than that of pure URu_2Si_2. We take this as an indication that something else, in addition to chemical pressure, must drive the ground state properties and f-electron count.

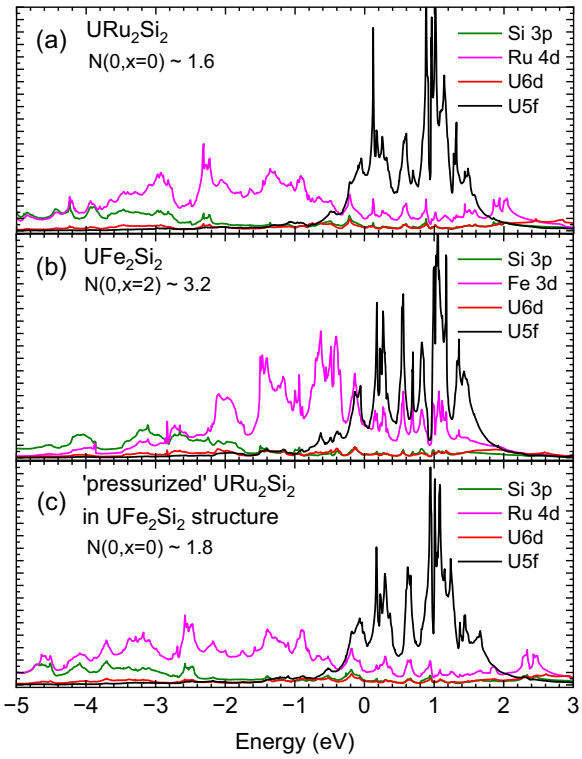

FIG. 6. Partial densities of states (DOSs) of (a) URu_2Si_2, (b) UFe_2Si_2, and (c) URu_2Si_2 in the structure of UFe_2Si_2 to mimic the effect of pressure. $N(0, x)$, where x is Fe content, is the sum of the partial DOS of the conduction electron states at the Fermi energy E_F, averaged on a 25 meV interval around E_F.

Figures 6(a) and 6(b) show the partial densities of states (DOSs) of URu_2Si_2 and UFe_2Si_2. The calculations were performed with the full-potential local-orbital (FPLO) code, employing the local density approximation (LDA) in a fully relativistic approach. A grid of $18 \times 18 \times 18$ k points and about one energy point every 8 meV is used in the calculation of the partial DOS. The magenta lines represent the transition metal d states. It is evident that the partial DOS changes significantly from Ru to Fe despite the isoelectronic character of the substitution; $N(0, x)$, the sum of the partial DOSs of the conduction electron states at the Fermi energy, doubles (see Fig. 6) from $x = 0$ to $x = 2$. In contrast, the partial DOS of URu_2Si_2 is hardly affected by pressure, as the comparison with Fig. 6(c) confirms. It shows the same calculation as in Fig. 6(a) but with the lattice parameters of UFe_2Si_2 in order to mimic only the pressure effect. For URu_2Si_2 with pressure, $N(0)$ hardly changes with respect to the value for ambient pressure URu_2Si_2. Hence, substitution has the additional effect of changing the density of states at the Fermi level, which we express in terms of the number $N(0, x)$.

The density of states at the Fermi level enters the expression of the Kondo temperature

$$T_K \propto \exp\left(-\frac{1}{N_f N(0,x)\mathcal{J}}\right). \tag{2}$$

Here, T_K is defined as in the large-N_f expansion [76,77] with $N_f = 2$, the degeneracy of the quasidoublet ground state provided that the splitting of the latter is smaller than T_K. T_K decreases with decreasing $\mathcal{J}$, but it increases with increasing $N(0, x)$. Indeed, for large x the material is Pauli paramagnetic, showing that T_K, due to the now dominating impact of $N(0, x)$, increases so much that the magnetic order is suppressed. A more dominating Kondo regime with respect to the magnetic regime suggests that the critical exchange interaction $\mathcal{J}_c$ at the QCP has moved to smaller values. $\mathcal{J}_c$ is now also a function of the Fe concentration x. Hence, the standard Doniach phase diagram is no longer sufficient. It now requires x as a third dimension [see Fig. 5(b)]. With a simple *heuristic* argument it can be shown that the QCP moves on a concave line, as shown by the black line in the $(x, \mathcal{J})$ plane in Fig. 5(b) (see Appendix A). The colored line in Fig. 5(b) indicates a possible path for $URu_{2-x}Fe_xSi_2$ across the phase diagram, given that, as reasoned above, the system is first antiferromagnetic and, eventually, Pauli paramagnetic.

What do the above considerations imply for the filling of the $5f$ shell that we see materialized in the satellite strength? Following, e.g., Fulde [78], n_f, expressed as the ratio of T_K and T_{RKKY}, represents the competing effects of the pressure and density of states. Here, we recall that

$$T_{\mathrm{RKKY}} \propto \mathcal{J}^2 N(0, x). \tag{3}$$

For small x, the $N(0, x)$ effect is not yet global because not every U atom has an Fe atom as the nearest neighbor. Here, pressure and the consequent decrease of $\mathcal{J}$ are the dominant effects, stabilizing the f^2 configuration and decreasing n_f (satellite increases). Eventually, for $x > 1.2$, i.e., when the Pauli paramagnetic regime is reached, n_f has, indeed, increased (satellite decreased) because now the density of states effect acts on all U atoms, thus causing the Kondo effect to overrule the magnetic ordering. The peculiar behavior in the interim section with the red arrows [Fig. 5(a)] may show that the pressure effect is still not negligible with respect to the growing density of states effect. It could also be due to the fact that the Néel temperature is still increasing up to $x \approx 1$.

C. Induced magnetism in the presence of a singlet ground state

It has not yet been discussed why the Néel temperature increases up to $x \approx 1$ despite the decrease in the magnetic moments beyond $x = 0.1$ [39]. This brings up the question of how magnetic order can form at all in the presence of a singlet or quasidoublet state consisting of the two singlet states $\Gamma_1^{(1)}(\theta) = \frac{1}{\sqrt{2}}\sin\theta(|+4\rangle + |-4\rangle) + \frac{1}{\sqrt{2}}\cos\theta|0\rangle$ and $\Gamma_2 = \frac{1}{\sqrt{2}}(|+4\rangle - |-4\rangle)$, neither of which carries a local magnetic moment. It should be mentioned that the dynamical mean field theory (DMFT) calculations by Haule and Kotliar found the same states to have the largest weight in the DMFT density matrix [10,11]. These authors further stated that these two states are compatible with antiferromagnetic order as well as hexadecapole order. Hence, the HO-LMAFM instability upon application of pressure or substitution may also be seen as the competition of these two order parameters.

A moment in the presence of a quasidoublet consisting of two singlet states can be acquired spontaneously below the ordering or critical temperature T_c only by coupling these two singlet states via intersite exchange $I_e \sim T_{\mathrm{RKKY}}$; that is, for *induced order* to occur there has to be a nonzero matrix element $\alpha = \langle \mathrm{gs}|J_z|\mathrm{es}\rangle$ between the singlet ground state $|\mathrm{gs}\rangle$ and the excited state $|\mathrm{es}\rangle$. The material orders magnetically below T_c

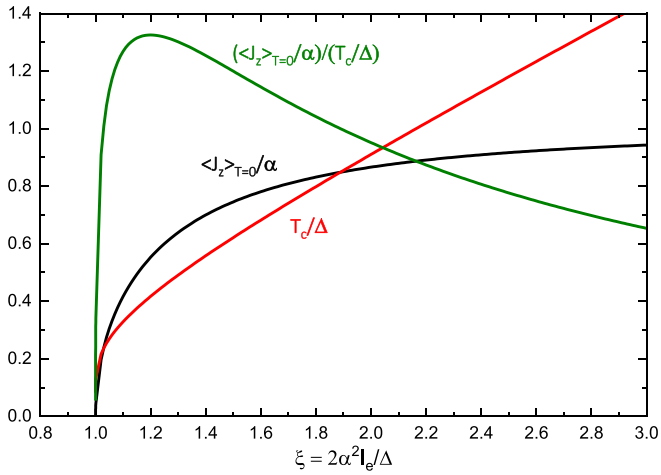

FIG. 7. Normalized saturation $\langle J_z\rangle_{T=0}$ and ordering temperature T_C as a function of the control parameter ξ for a singlet-singlet system.

when the control parameter ξ is larger than 1 [71,79], where ξ depends on the ratio of the intersite exchange interaction I_e and the energy difference of the two singlet states Δ times the square of the matrix element α (see Appendix B). For $\xi > 1$, the quasidoublet $\Gamma_1^{(1)}$-Γ_2 may carry any magnetic moment between 0 and $4g_J\mu_B$ along the tetragonal c axis. Moreover, it is natural for induced moment magnetism that the ordered moment saturates while the corresponding critical temperature still increases (see Fig. 1) in the limit of large control parameters where they asymptotically approach the conventional behavior of a magnet with a Kramers doublet ground state. In order to illustrate such a trend, we show in Fig. 7 the magnetic moment $\langle J_z\rangle_{T=0}/\alpha$, the critical temperature T_c/Δ, and their ratio $(\langle J_z\rangle_{T=0}/\alpha)/(T_c/\Delta)$ as a function of the control parameter ξ in the singlet-singlet model. This dependence is reminiscent of the T-x phase diagram of $URu_{2-x}Fe_xSi_2$ in the low-doping regime where $\mu_{\rm ord}$ reaches its maximum value while T_N continues to increase (see Fig. 1). The presence of a sufficiently strong Kondo-type interaction will destroy such induced order; that is, the Doniach concept is also applicable for induced order.

The induced character of the magnetic order introduces two more parameters, namely, the dipolar matrix element α and the energy splitting Δ between the two singlet states forming the quasidoublet, that may change with the Fe concentration x. This may contribute to the formation of magnetic order despite the larger degree of itinerancy in the interim doping regime.

V. CONCLUDING REMARKS

The substitution series $URu_{2-x}Fe_xSi_2$ was investigated with $4f$ core-level photoelectron spectroscopy, and nonmonotonic shifts of spectral weight were observed. The initial increase and subsequent decrease in the satellite intensities of the U $4f$ core level with x were interpreted in terms of two competing effects: chemical pressure stabilizing the f^2 configuration and hence magnetic order and the increase in the density of states at the Fermi energy enhancing the number of itinerant electrons. This was captured in an extended Doniach phase diagram with a $(\mathcal{J}, x)$ plane in addition to the standard $(T, \mathcal{J})$ plane and a quantum critical point moving as function of the Fe concentration x. The discussion in terms of a Doniach phase diagram is possible because it was confirmed that URu_2Si_2, UFe_2Si_2, and also the substitution series have the same ground state symmetry, namely, a singlet or quasidoublet state. Finally, the formation of magnetic order was discussed in terms of singlet magnetism.

ACKNOWLEDGMENTS

This research was carried out at the National Synchrotron Radiation Research Centre (NSRRC) in Taiwan and at PETRA III/DESY, a member of the Helmholtz Association HGF. Research at the University of California, San Diego, was supported by the U.S. Department of Energy, Office of Science, Basic Energy Sciences, under Grant No. DEFG02-04-ER45105 (single-crystal growth) and the U.S. National Science Foundation under Grant No. DMR-1810310 (materials characterization). A.A. and A.S. gratefully acknowledge the financial support of the Deutsche Forschungsgemeinschaft under Project No. 387555779. All authors thank H. Hess from the Institute of Nuclear Physics at the University of Cologne for providing the γ spectra of the uranium samples and the Max Planck-POSTECH-Hsinchu Center for Complex Phase Materials for support.

APPENDIX A: DONIACH PHASE DIAGRAM HEURISTICS

The relevant scales within the Doniach phase diagram approach are the Kondo and Ruderman-Kittel-Kasuya-Yosida (RKKY) interactions, whose characteristic energy scales are respectively given by

$$T_K(x) = \frac{1}{\rho(x)}\exp\left(-\frac{1}{N_f\rho(x)\mathcal{J}(x)}\right), \tag{A1}$$

$$T_{\rm RKKY}(x) = \mathcal{J}(x)^2\rho(x), \tag{A2}$$

where x is the Fe concentration, $N_f = 2$ is the degeneracy of the quasidoublet ground state, $\rho(x) = N(0, x)$ is the density of conduction states at the Fermi level, and $\mathcal{J}(x)$ is the on-site exchange coupling. Let us define

$$\tilde{g}(x) = \mathcal{J}(x)\rho(x). \tag{A3}$$

At the quantum critical point the condition $T_{\rm RKKY} = T_K$ holds, which means in terms of the quantum critical $\tilde{g}_c(x)$:

$$\tilde{g}_c(x)^2 = \exp\left(-\frac{1}{2\tilde{g}_c(x)}\right). \tag{A4}$$

This equation has the same solution $\tilde{g}(x) = \text{const}(= 0.12 \ll 1)$ for all x. In other words,

$$\tilde{g}_c(x) = \text{const} = \tilde{g}_c(0), \tag{A5}$$

$$\mathcal{J}_c(x)\rho_c(x) = \mathcal{J}(0)\rho(0). \tag{A6}$$

From Eq. (A6) we can see that $\mathcal{J}_c$ is inversely proportional to the density of states at the Fermi level $\rho_c(x)$. Assuming that the latter increases monotonically with x, this behavior is indicated by the concavity of the black line in Fig. 5(b) in the main text.

APPENDIX B: INDUCED ORDER FOR SINGLET-SINGLET SYSTEM

We consider here a system with a singlet ground state $|\mathrm{gs}\rangle$ and a singlet first excited state $|\mathrm{es}\rangle$ with energy splitting Δ and an ordered magnetic moment along the c axis as in the LMAFM phase of $URu_{2-x}Fe_xSi_2$. Singlets do not carry a magnetic moment by themselves, i.e., $\langle \mathrm{gs}|J_z|gs\rangle = 0$, so the magnetism cannot originate from the ordering of local magnetic moments that also exist above the critical temperature T_c, as in an ordinary magnet. However, an induced type of order may occur if a nonvanishing matrix element $\alpha = \langle gs|J_z|es\rangle$ that couples the ground state and excited state singlets exists. The magnetic properties of the system can then be characterized by the control parameter:

$$\xi = 2\frac{\alpha^2 I_e}{\Delta}. \tag{B1}$$

For the derivation the reader is referred to [71,79]. Here, we report only the main results in brief as a service to the reader. The critical temperature T_c and the saturation moment $\langle J_z\rangle_{T=0}$ can be written as

$$T_c = \frac{\Delta}{2\tanh^{-1}\frac{1}{\xi}}, \tag{B2}$$

$$\langle J_z\rangle_{T=0} = \alpha\frac{1}{\xi}(\xi^2-1)^{\frac{1}{2}}. \tag{B3}$$

For $\xi > 1$, a spontaneous moment can form, and for $\xi \gg 1$, this moment is as large as α, i.e., $\langle J_z\rangle_{T=0} = \alpha$. When the two singlets in question are $\Gamma_1^{(1)}(\theta) = \frac{1}{\sqrt{2}}\sin\theta(|+4\rangle + |-4\rangle) + \frac{1}{\sqrt{2}}\cos\theta|0\rangle$ and $\Gamma_2 = \frac{1}{\sqrt{2}}(|+4\rangle - |-4\rangle)$, then we find $\alpha = 4\sin\theta$, implying the material in question can have up to $\langle J_z\rangle_{T=0} = 4\sin\theta$, i.e., magnetic moments as large as $4g_J\sin\theta$ in μ_B, thus accommodating even the large ordered moments of UPd_2Si_2 [62,63] and UNi_2Si_2 [64].

[1] T. T. M. Palstra, A. A. Menovsky, J. van den Berg, A. J. Dirkmaat, P. H. Kes, G. J. Nieuwenhuys, and J. A. Mydosh, Phys. Rev. Lett. **55**, 2727 (1985).

[2] W. Schlabitz, J. Baumann, B. Pollit, U. Rauchschwalbe, H. M. Mayer, U. Ahlheim, and C. D. Bredl, Z. Phys. B **62**, 171 (1986).

[3] M. B. Maple, J. W. Chen, Y. Dalichaouch, T. Kohara, C. Rossel, M. S. Torikachvili, M. W. McElfresh, and J. D. Thompson, Phys. Rev. Lett. **56**, 185 (1986).

[4] P. M. Oppeneer, J. Rusz, S. Elgazzar, M.-T. Suzuki, T. Durakiewicz, and J. A. Mydosh, Phys. Rev. B **82**, 205103 (2010).

[5] J. A. Mydosh and P. M. Oppeneer, Rev. Mod. Phys. **83**, 1301 (2011).

[6] J. A. Mydosh and P. M. Oppeneer, Philos. Mag. **94**, 3642 (2014).

[7] J. A. Mydosh, P. M. Oppeneer, and P. S. Riseborough, J. Phys.: Condens. Matter **32**, 143002 (2020).

[8] C. Broholm, J. K. Kjems, W. J. L. Buyers, P. Matthews, T. T. M. Palstra, A. A. Menovsky, and J. A. Mydosh, Phys. Rev. Lett. **58**, 1467 (1987).

[9] P. G. Niklowitz, C. Pfleiderer, T. Keller, M. Vojta, Y.-K. Huang, and J. A. Mydosh, Phys. Rev. Lett. **104**, 106406 (2010).

[10] K. Haule and G. Kotliar, Nat. Phys. **5**, 796 (2009).

[11] K. Haule and G. Kotliar, Europhys. Lett. **89**, 57006 (2010).

[12] H. Kusunose and H. Harima, J. Phys. Soc. Jpn. **80**, 084702 (2011).

[13] H.-H. Kung, R. E. Baumbach, E. D. Bauer, V. K. Thorsmølle, W.-L. Zhang, K. Haule, J. A. Mydosh, and G. Blumberg, Science **347**, 1339 (2015).

[14] H. Ikeda, M.-T. Suzuki, R. Arita, T. Takimoto, T. Shibauchi, and Y. Matsuda, Nat. Phys. **8**, 528 (2012).

[15] P. Thalmeier, T. Takimoto, and H. Ikeda, Philos. Mag. **94**, 3863 (2014).

[16] R. Okazaki, T. Shibauchi, H. J. Shi, Y. Haga, T. D. Matsuda, E. Yamamoto, Y. Onuki, H. Ikeda, and Y. Matsuda, Science **331**, 439 (2011).

[17] S. Kambe, Y. Tokunaga, H. Sakai, T. Hattori, N. Higa, T. D. Matsuda, Y. Haga, R. E. Walstedt, and H. Harima, Phys. Rev. B **97**, 235142 (2018).

[18] J. Flouquet, Prog. Low Temp. Phys. **15**, 139 (2005).

[19] P. Thalmeier and G. Zwicknagl, in *Handbook on the Physics and Chemistry of Rare Earths*, edited by J.-C. B. K. A. Gschneidner, Jr. and V. Pecharsky (Elsevier, Amsterdam, 2005), Vol. 34, pp. 139–268.

[20] P. Coleman, in *Handbook of Magnetism and Advanced Magnetic Materials* (Wiley, Hoboken, NJ, 2007), pp. 95–148.

[21] H. v. Löhneysen, A. Rosch, M. Vojta, and P. Wölfle, Rev. Mod. Phys. **79**, 1015 (2007).

[22] D. I. Khomskii, *Basic Aspects of the Quantum Theory of Solids* (Cambridge University Press, Cambridge, 2010).

[23] O. Stockert, S. Kirchner, F. Steglich, and Q. Si, J. Phys. Soc. Jpn. **81**, 011001 (2012).

[24] B. White, J. Thompson, and M. Maple, Phys. C (Amsterdam, Neth.) **514**, 246 (2015).

[25] P. Coleman, *Introduction to Many-Body Physics* (Cambridge University Press, Cambridge, 2015).

[26] P. Santini and G. Amoretti, Phys. Rev. Lett. **73**, 1027 (1994).

[27] P. Santini, Phys. Rev. B **57**, 5191 (1998).

[28] M. Sundermann, M. W. Haverkort, S. Agrestini, A. Al-Zein, M. Moretti Sala, Y. Huang, M. Golden, A. de Visser, P. Thalmeier, L. H. Tjeng, and A. Severing, Proc. Natl. Acad. Sci. USA **113**, 13989 (2016).

[29] A. Amorese, M. Sundermann, B. Leedahl, A. Marino, D. Takegami, H. Gretarsson, A. Gloskovskii, C. Schlueter, M. W. Haverkort, Y. Huang, M. Szlawska, D. Kaczorowski, S. Ran, M. B. Maple, E. D. Bauer, A. Leithe-Jasper, P. Hansmann, P. Thalmeier, L. H. Tjeng, and A. Severing, Proc. Natl. Acad. Sci. USA **117**, 30220 (2020).

[30] H. Amitsuka, M. Sato, N. Metoki, M. Yokoyama, K. Kuwahara, T. Sakakibara, H. Morimoto, S. Kawarazaki, Y. Miyako, and J. A. Mydosh, Phys. Rev. Lett. **83**, 5114 (1999).

[31] F. Bourdarot, A. Bombardi, P. Burlet, M. Enderle, J. Flouquet, P. Lejay, N. Kernavanois, V. Mineev, L. Paolasini, M. Zhitomirsky, and B. Fåk, Phys. B (Amsterdam, Neth.) **359–361**, 986 (2005).

[32] H. Amitsuka, K. Matsuda, I. Kawasaki, K. Tenya, M. Yokoyama, C. Sekine, N. Tateiwa, T. Kobayashi, S. Kawarazaki, and H. Yoshizawa, J. Magn. Magn. Mater. **310**, 214 (2007).

[33] N. P. Butch, J. R. Jeffries, S. Chi, J. B. Leão, J. W. Lynn, and M. B. Maple, Phys. Rev. B **82**, 060408(R) (2010).

[34] J. Choi, O. Ivashko, N. Dennler, D. Aoki, K. von Arx, S. Gerber, O. Gutowski, M. H. Fischer, J. Strempfer, M. v. Zimmermann, and J. Chang, Phys. Rev. B **98**, 241113(R) (2018).

[35] Y. Dalichaouch, M. B. Maple, M. S. Torikachvili, and A. L. Giorgi, Phys. Rev. B **39**, 2423 (1989).

[36] H. Amitsuka, K. Hyomi, T. Nishioka, Y. Miyako, and T. Suzuki, J. Magn. Magn. Mater. **76–77**, 168 (1988).

[37] M. Yokoyama, H. Amitsuka, S. Itoh, I. Kawasaki, K. Tenya, and H. Yoshizawa, J. Phys. Soc. Jpn. **73**, 545 (2004).

[38] K. Prokeš, Y.-K. Huang, M. Reehuis, B. Klemke, J.-U. Hoffmann, A. Sokolowski, A. de Visser, and J. A. Mydosh, Phys. Rev. B **95**, 035138 (2017).

[39] P. Das, N. Kanchanavatee, J. S. Helton, K. Huang, R. E. Baumbach, E. D. Bauer, B. D. White, V. W. Burnett, M. B. Maple, J. W. Lynn, and M. Janoschek, Phys. Rev. B **91**, 085122 (2015).

[40] T. J. Williams, A. A. Aczel, M. B. Stone, M. N. Wilson, and G. M. Luke, Phys. Rev. B **95**, 104440 (2017).

[41] N. Kanchanavatee, M. Janoschek, R. E. Baumbach, J. J. Hamlin, D. A. Zocco, K. Huang, and M. B. Maple, Phys. Rev. B **84**, 245122 (2011).

[42] M. N. Wilson, T. J. Williams, Y.-P. Cai, A. M. Hallas, T. Medina, T. J. Munsie, S. C. Cheung, B. A. Frandsen, L. Liu, Y. J. Uemura, and G. M. Luke, Phys. Rev. B **93**, 064402 (2016).

[43] N. P. Butch, S. Ran, I. Jeon, N. Kanchanavatee, K. Huang, A. Breindel, M. B. Maple, R. L. Stillwell, Y. Zhao, L. Harriger, and J. W. Lynn, Phys. Rev. B **94**, 201102(R) (2016).

[44] S. Ran, C. T. Wolowiec, I. Jeon, N. Pouse, N. Kanchanavatee, B. D. White, K. Huang, D. Martien, T. DaPron, D. Snow, M. Williamsen, S. Spagna, P. S. Riseborough, and M. B. Maple, Proc. Natl. Acad. Sci. USA **113**, 13348 (2016).

[45] C. T. Wolowiec, N. Kanchanavatee, K. Huang, S. Ran, and M. B. Maple, Phys. Rev. B **94**, 085145 (2016).

[46] H.-H. Kung, S. Ran, N. Kanchanavatee, V. Krapivin, A. Lee, J. A. Mydosh, K. Haule, M. B. Maple, and G. Blumberg, Phys. Rev. Lett. **117**, 227601 (2016).

[47] S. Ran, I. Jeon, N. Pouse, A. J. Breindel, N. Kanchanavatee, K. Huang, A. Gallagher, K.-W. Chen, D. Graf, R. E. Baumbach, J. Singleton, and M. B. Maple, Proc. Natl. Acad. Sci. USA **114**, 9826 (2017).

[48] P. Kissin, S. Ran, D. Lovinger, V. K. Thorsmølle, N. Kanchanavatee, K. Huang, M. B. Maple, and R. D. Averitt, Phys. Rev. B **99**, 165144 (2019).

[49] Y. Dalichaouch, M. B. Maple, J. W. Chen, T. Kohara, C. Rossel, M. S. Torikachvili, and A. L. Giorgi, Phys. Rev. B **41**, 1829 (1990).

[50] N. Kanchanavatee, B. White, V. Burnett, and M. Maple, Philos. Mag. **94**, 3681 (2014).

[51] C. T. Wolowiec, N. Kanchanavatee, K. Huang, S. Ran, A. J. Breindel, N. Pouse, K. Sasmal, R. E. Baumbach, G. Chappell, P. S. Riseborough, and M. B. Maple, Proc. Natl. Acad. Sci. USA **118**, e2026591118 (2021).

[52] K.-H. J. Buschow and D. B. de Mooij, Philips J. Research **41**, 55 (1986).

[53] T. T. Palstra, A. A. Menovsky, G. J. Nieuwenhuys, and J. A. Mydosh, J. Magn. Magn. Mater. **54–57**, 435 (1986).

[54] A. Szytuka, S. Siek, J. Leciejewicz, A. Zygmunt, and Z. Ban, J. Phys. Chem. Solids **49**, 1113 (1988).

[55] T. Endstra, S. A. M. Mentink, G. J. Nieuwenhuys, and J. A. Mydosh, in *Selected Topics in Magnetism*, edited by L. C. Gupta and M. Multani (World Scientific, Singapore, 1993), Vol. 2. p. 460.

[56] T. Endstra, G. J. Nieuwenhuys, and J. A. Mydosh, Phys. Rev. B **48**, 9595 (1993).

[57] E. Frantzeskakis, J. Dai, C. Bareille, T. C. Rödel, M. Güttler, S. Ran, N. Kanchanavatee, K. Huang, N. Pouse, C. T. Wolowiec, E. D. L. Rienks, P. Lejay, F. Fortuna, M. B. Maple, and A. F. Santander-Syro, Proc. Natl. Acad. Sci. USA **118**, e2020750118 (2021).

[58] O. Gunnarsson and K. Schönhammer, Phys. Rev. B **28**, 4315 (1983).

[59] F. de Groot, J. Electron Spectrosc. Relat. Phenom. **67**, 529 (1994).

[60] S. Fujimori, Y. Saito, N. Sato, T. Komatsubara, S. Suzuki, S. Sato, and T. Ishii, Solid State Commun. **105**, 185 (1998).

[61] S.-I. Fujimori, Y. Takeda, T. Okane, Y. Saitoh, A. Fujimori, H. Yamagami, Y. Haga, E. Yamamoto, and Y. Ōnuki, J. Phys. Soc. Jpn. **85**, 062001 (2016).

[62] H. Ptasiewicz-Bak, J. Leciejewicz, and A. Zygmunt, J. Phys. F **11**, 1225 (1981).

[63] B. Shemirani, H. Lin, M. F. Collins, C. V. Stager, J. D. Garrett, and W. J. L. Buyers, Phys. Rev. B **47**, 8672 (1993).

[64] H. Lin, L. Rebelsky, M. F. Collins, J. D. Garrett, and W. J. L. Buyers, Phys. Rev. B **43**, 13232 (1991).

[65] H.-M. Tsai, H.-W. Fu, C.-Y. Kuo, L.-J. Huang, C.-S. Lee, C.-Y. Hua, K.-Y. Kao, H.-J. Lin, H.-S. Fung, S.-C. Chung, C.-F. Chang, A. Chainani, L. H. Tjeng, and C.-T. Chen, in *Proceedings of the 13th International Conference on Synchrotron Radiation Instrumentation – SRI2018*, AIP Conf. Proc. No. 2054 (AIP, Melville, NY, 2019), p. 060047.

[66] M. Sundermann, K. Chen, H. Yavaş, H. Lee, Z. Fisk, M. W. Haverkort, L. H. Tjeng, and A. Severing, Europhys. Lett. **117**, 17003 (2017).

[67] W. Schükle, *Electron Dynamics by Inelastic X-Ray Scattering* (Oxford Science Publications, Oxford, 2007).

[68] M. W. Haverkort, A. Tanaka, L. H. Tjeng, and G. A. Sawatzky, Phys. Rev. Lett. **99**, 257401 (2007).

[69] R. Caciuffo, G. van der Laan, L. Simonelli, T. Vitova, C. Mazzoli, M. A. Denecke, and G. H. Lander, Phys. Rev. B **81**, 195104 (2010).

[70] M. Sundermann, G. van der Laan, A. Severing, L. Simonelli, G. H. Lander, M. W. Haverkort, and R. Caciuffo, Phys. Rev. B **98**, 205108 (2018).

[71] P. Thalmeier, Eur. Phys. J. B **27**, 29 (2002).

[72] G. Zwicknagl and P. Fulde, J. Phys.: Condens. Matter **15**, S1911 (2003).

[73] J. Lee, M. Matsuda, J. A. Mydosh, I. Zaliznyak, A. I. Kolesnikov, S. Süllow, J. P. C. Ruff, and G. E. Granroth, Phys. Rev. Lett. **121**, 057201 (2018).

[74] J. R. Schrieffer and P. A. Wolff, Phys. Rev. **149**, 491 (1966).

[75] H. Okamura, A. Takigawa, T. Yamasaki, E. D. Bauer, S. Ohara, Y. Ikemoto, and T. Moriwaki, Phys. Rev. B **100**, 195112 (2019).

[76] N. E. Bickers, D. L. Cox, and J. W. Wilkins, Phys. Rev. B **36**, 2036 (1987).

[77] D. Newns and N. Read, Adv. Phys. **36**, 799 (1987).

[78] P. Fulde, *Electron Correlations in Molecules and Solids* (Springer, Berlin, 1995), Vol. 2.

[79] P. Thalmeier, Phys. Rev. B **103**, 144435 (2021).